JMEPEG (2008) 17:879–887
DOI: 10.1007/s11665-008-9212-x

1059-9495/$19.00

Effect of Residual Stress on Fatigue Failure of Carbonitrided Low-Carbon Steel

C. Kanchanomai and W. Limtrakarn

(Submitted April 19, 2007; in revised form December 10, 2007)

The effect of residual stress on fatigue behavior and mechanisms of carbonitrided AISI 1015 steel under uniaxial cyclic loading has been experimentally studied. By progressive removal of thin surface layers using an electropolishing technique and subsequent residual stress measurements using an x-ray diffraction technique, the compressive residual stress at the surface was approximately 900 MPa. The stress decreased toward the center, and became stable tensile residual stress of approximately 20 MPa. The fatigue resistance of carbonitrided AISI 1015 steel was higher than that of AISI 1015 steel due to the presence of compressive residual stress in case layer. The fatigue limit of AISI 1015 steels with and without carbonitriding was 340 and 300 MPa, respectively. Subsurface cracks initiated at the case-core interface, i.e. approximately 400 μm from the surface. With increasing number of stress cycles, the subsurface cracks coalesced and propagated intergranularly through the case layer. After some incubation cycles, the subsurface cracks reached the surface of specimen, and became a main crack. During this stage, the stress increased, and caused the formation of voids in core material. Consequently, the crack propagated through the core material, interacted with voids, and caused complete fracture.

Keywords AISI 1015 steel, carbonitriding, fatigue, low-carbon steel, residual stress

1. Introduction

Due to safety, economic, and environmental reasons, significant amounts of effort have been spent to extend the service life of machine components and structures. To meet these demands, various surface modification technologies have become major interest because they can provide superior surface properties such as high strength, thermal barrier, corrosion resistance, wear resistance, and fatigue resistance to structural materials. For high-alloy steels, an increase in fatigue resistance after various thermochemical heat treatments has been reported (Ref 1-5), while only a few studies have been done on low-carbon steels. Since the low-carbon steels have excellent ductility and fracture toughness, various machining processes could be preformed with fewer defects. With the ability to modify the strength, corrosion resistance, wear resistance, and fatigue resistance of low-carbon steels by thermochemical heat treatments, the surface properties of parts after machining could be improved and used for engineering applications, e.g. gear drives, pump shafts, and guide bars (Ref 5).

It is known that the tensile mean stress reduces the fatigue resistance, while the compressive mean stress improves the fatigue resistance. The compressive mean stress can often be achieved by introducing residual stress, i.e. the stresses remain in the part from previous operation. Using thermochemical heat treatment, the surface skin or case becomes harder and the compressive residual stress can reach the yield strength, while the tensile residual stress occurs in the core to maintain the force equilibrium within the part. For the materials under rotating bending, the maximum applied tensile stress is on the outer surface. The stress decreases, and become zero at neutral axis. With the introduction of thermochemical heat treatment, the formation and propagation of surface cracks can be retarded by the compressive residual stress around the surface; therefore, the fatigue resistance of the parts under rotating bending is significantly improved. Unlike the materials under rotating bending, the applied tensile stress of materials under uniaxial cyclic loading is not decreased with the distance from the surface. With the introduction of thermochemical heat treatment, the applied tensile stress can superpose with the tensile residual stress in core, and results in the formation and propagation of subsurface cracks. The improvement of fatigue resistance of the parts under uniaxial cyclic loading by using thermochemical heat treatment is therefore less than that under rotating bending (Ref 6, 7).

The effect of hard layer thickness on low-cycle and high-cycle fatigue properties of carburized AISI 8620 steel using rotating bending tests has been studied by Farfan et al. (Ref 8). They found that the greater the case depth the higher the fatigue strength, and the fracture mechanisms were the combination of brittle fracture in the hard layer and ductile fracture in the core of specimen. Karadog and Stephens (Ref 9) have conducted the high-tensile mean stress fatigue tests for R ratios of 0.8 and 0.9 on unnotched SAE 1045 steel uniaxial fatigue specimens with various hardness levels (10, 37, and 50 R_c). At high R ratios, the fatigue strength based on maximum stress was higher than that at low-R ratios. Cyclic creep/ratcheting was present for all three hardness levels; however, R_c = 10 and 37 had significantly

C. Kanchanomai and **W. Limtrakarn**, Department of Mechanical Engineering, Faculty of Engineering, Thammasat University, Klong-Luang, Pathumthani 12120, Thailand. Contact e-mail: kchao@engr.tu.ac.th.

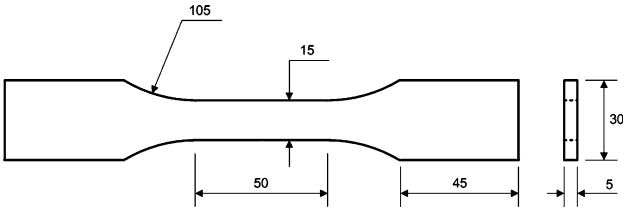

Fig. 1 Geometry of the fatigue specimen (dimension in mm)

more cyclic creep/ratcheting than $R_c = 50$. Both $R_c = 10$ and 37 monotonic and cyclic specimens fractured in a ductile manner with cup-cone shaped final fracture, where internal microvoid coalescence (ductile dimples) was dominant with small amounts of microcleavage. The $R_c = 50$ cyclic specimens fractured in a brittle manner involving less cyclic creep/ratcheting. Using four-point bending tests, McEvily et al. (Ref 10) found that the cracks of carburized AISI 9310 steel under monotonic and cyclic loading initiated from the case-core interface due to the radial tensile stress from the mismatch of deformation between case-core materials. Genel et al. (Ref 11) found that the cracks of ion-nitrided AISI 4140 steel under cyclic loading initiated from inclusions which formed fish eye mark on the fracture surface, and the fatigue life from rotary bending fatigue tests improved with increasing case depth.

As a modification of gas carburizing, carbonitriding is a process of adding ammonia into the gas-carburizing atmosphere, i.e. both nitrogen and carbon can be introduced into the steel. It can be performed for low-carbon steels under lower temperature and shorter time than carburizing process; therefore, it obtains similar hardness with less distortion (Ref 5). The hardness and tribological properties of the low-carbon steel treated by carbonitriding were superior to those of low-carbon steel without any treatment and with carburizing (Ref 12). Even the carbonitriding of low-carbon steels is being used in engineering applications, only limited work has been done on their fatigue behavior and mechanisms, especially under uniaxial cyclic loading. It was the objective of the present work to study the fatigue failure of carbonitrided low-carbon steel under uniaxial cyclic loading. The influence of residual stress on fatigue life was evaluated, and fatigue mechanisms were then discussed.

2. Materials and Experimental Procedures

From a plate of hot-rolled low-carbon steel, fatigue specimens were cut and machined using an NC milling machine. The configuration of the specimen, which was designed according to the ASTM E466-96 (Ref 13), is shown in Fig. 1. To avoid the complication due to the effect of rolling direction on fatigue properties, the longitudinal axis of specimen was set parallel to the rolling direction of steel plate. Carbonitriding process was carried out by preheating the specimens to 870 °C in an atmosphere of an endothermic gas for 30 min to ensure temperature uniformity. Subsequently, the enriching gas (1% carbon potential) and ammonia (NH_3) were introduced into the furnace with the flow rate of 18 m^3/h, and maintained at 870 °C for 180 min before quenching the specimens into oil at 60 °C. Tempering process was preformed by maintaining the specimens at 180 °C for 2 h, followed by air cooling before performing the tensile and fatigue tests. The specimens without carbonitriding were also annealed at 870 °C for 180 min, and cooled in air before performing the tensile and fatigue tests. The compositions of specimens with and without carbonitriding were analyzed by an emission spectrometer (Baird: Spectovac 2000 Arc/Spark). Since the ability to analyze the percentage of nitrogen is limited for the present emission spectrometer, only percentages of fundamental elements, e.g. C, Si, Mn, and P, were determined. The formation of carbon-iron and nitrogen-iron compounds after carbonitriding was evaluated using an X-ray diffractometer (Bruker-axs: D8 discover with Cu $K\alpha$ radiation). To reveal the microstructure, the specimen was sectioned transversely using an electric discharge machine (EDM), polished, etched with 2 mL of nitric acid and 98 mL of methanol, and then observed in an scanning electron microscope (SEM).

The residual stress profile in depth direction of carbonitrided specimen was obtained by progressive removals of thin surface layers using an electropolishing machine (Struer: LECtroPol-5), and subsequent residual stress measurements using an X-ray diffraction machine (Bruker-axs: D8 discover with Cu $K\alpha$ radiation). To remove approximately 70 μm surface layer, electropolishing was performed at 60 V-DC for 60 s at room temperature in a solution of ethanol (95%) 700 mL, 2-butoxy ethanol 100 mL and perchloric acid (30%) 200 mL (Ref 14). The x-ray diffraction technique for residual stress measurement was carried out in eight steps of the angle between the normal to the specimen surface and the normal to the diffractive surface (ψ), which covered the range of 0-52.5°. The residual stresses were then determined using the $\sin^2\psi$ method.

The mechanical properties of AISI 1015 steels with and without carbonitriding were evaluated by the microhardness test (Ref 15) and tensile test (Ref 16). The uniaxial load-controlled fatigue tests (Ref 13) were performed by using a servo-hydraulic fatigue machine (Instron 8801—100 kN load cell) under 55% relative humidity, and 25 °C temperature. A sinusoidal waveform with zero stress ratio (R) and frequency of 30 Hz was used for the fatigue tests. The cycle loading was started from tensile side. The fatigue failure was defined as complete fracture of specimen. Fracture surfaces of specimens were observed in an SEM, and the mechanisms of fatigue were discussed.

3. Results and Discussion

3.1 Composition, Microstructure, Mechanical Properties, and Residual Stress

The compositions of low-carbon steels with and without carbonitriding are listed in Table 1. The composition of the present low-carbon steel corresponded to that of AISI 1015 steel (Ref 17), while 0.6 wt.% of carbon was found at the surface of carbonitrided specimen. The x-ray diffraction patterns on the surface and 1000 μm below the surface of the carbonitrided specimen are shown in Fig. 2. The formation of carbon-iron and nitrogen-iron compounds was observed on the surface of carbonitrided specimen, while mainly iron was observed at 1000 μm below the surface of the carbonitrided specimen. The SEM micrographs of AISI 1015 steel and carbonitrided AISI 1015 steel at different distances from

Table 1 Composition of AISI 1015 steel and carbonitrided AISI 1015 steel (wt.%)

Material	C	Si	Mn	P	S	Cr	Ni	Al	Sn	Ti	Cu	Fe
AISI 1015 steel	0.152	0.221	0.392	0.008	0.011	0.030	0.029	0.009	0.001	0.007	0.045	Bal.
Carbonitrided AISI 1015 steel	0.624	0.270	0.336	0.022	0.007	0.071	0.060	0.003	0.011	0.007	0.215	Bal.

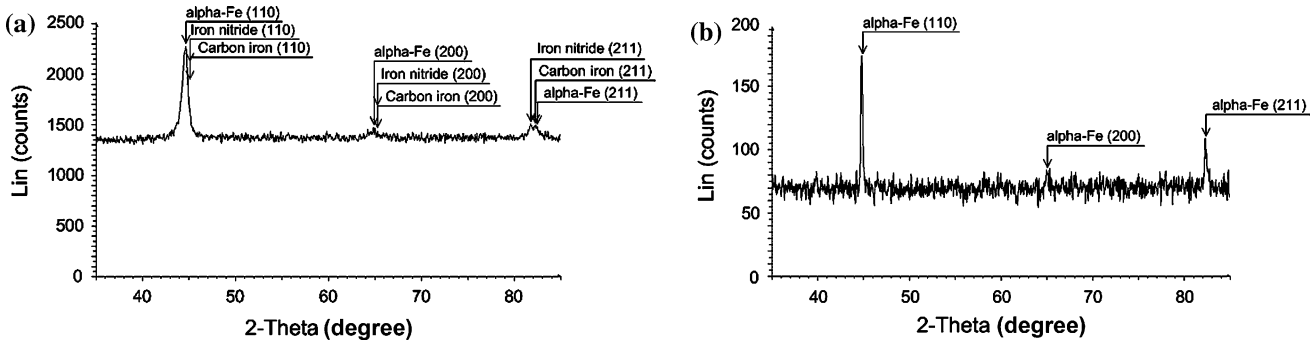

Fig. 2 X-ray diffraction patterns measured on; (a) the surface of the carbonitrided specimen, and (b) 1000 μm below the surface of carbonitrided specimen

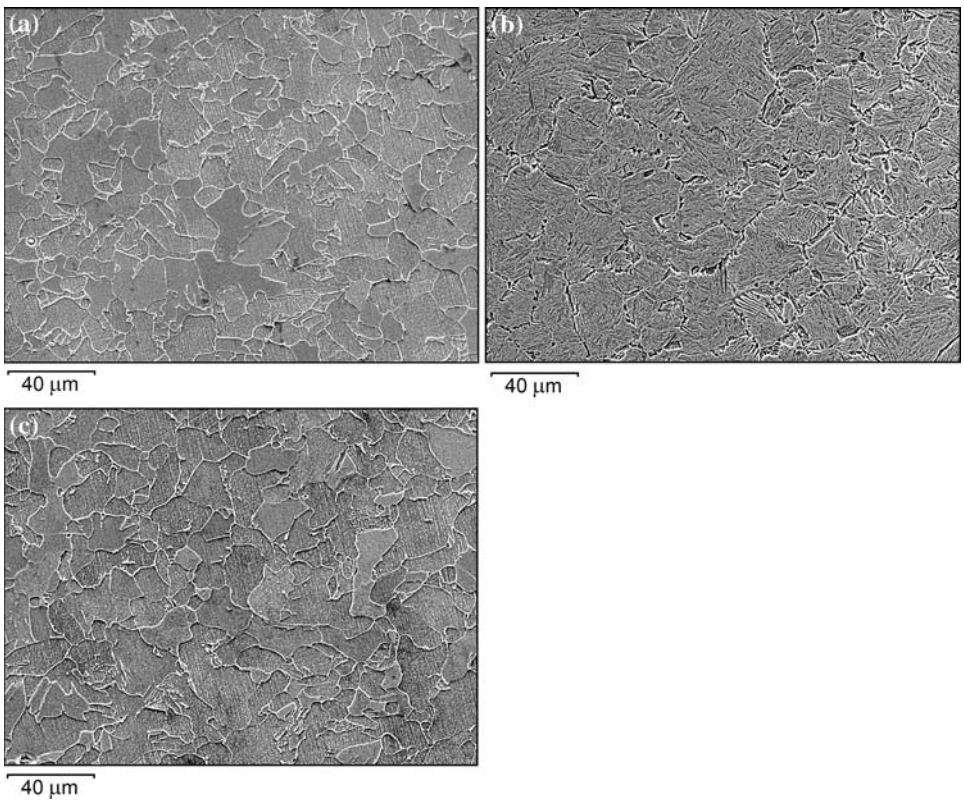

Fig. 3 SEM micrographs of; (a) AISI 1015 steel, (b) carbonitrided AISI 1015 steel at 100 μm below the surface, and (c) carbonitrided AISI 1015 steel at 1000 μm below the surface

surface are shown in Fig. 3(a)-(c). For AISI 1015 steel, ferrite was the major phase, while some pearlite could be observed. On the other hand, tempered martensite and retained austenite formed in the case layer of carbonitrided AISI 1015 steel (Fig. 3b). These phases decreased with increasing depth, and the microstructure became similar to that of AISI 1015 steel (Fig. 3c).

The microhardness tests were performed on the transverse section of specimens in four perpendicular directions. In each direction, the microhardness tests were performed three times. The variation of hardness was <5%, and the average hardness was determined. The relationship between the average hardness and the distance from surface of carbonitrided specimen is shown in Fig. 4. The hardness was high at the surface,

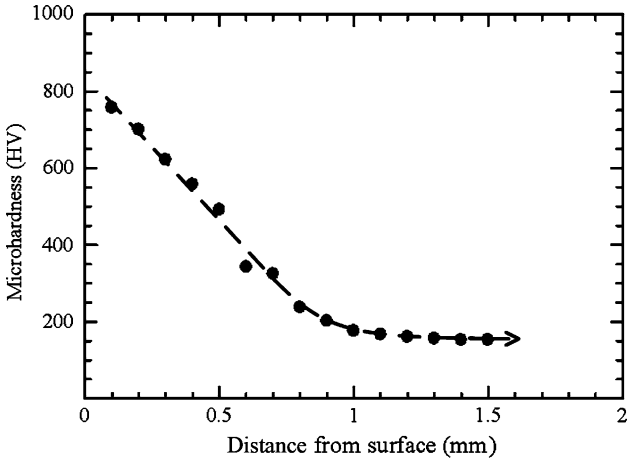

Fig. 4 Relationship between hardness and distance from the surface of carbonitrided AISI 1015 steel

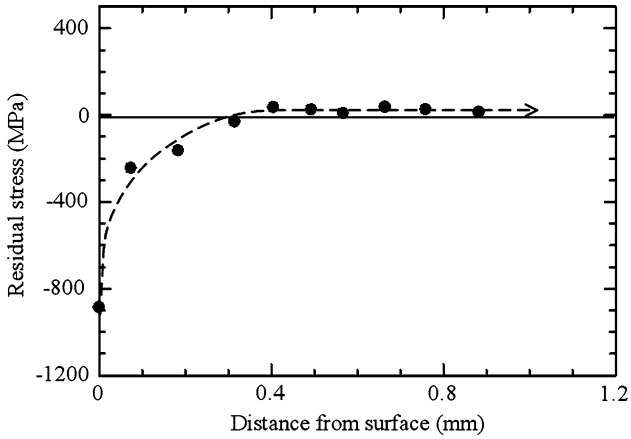

Fig. 5 Relationship between residual stress and distance from the surface of carbonitrided AISI 1015 steel

Table 2 Mechanical properties of AISI 1015 steels with and without carbonitriding

Mechanical properties	AISI 1015 steel	Carbonitrided AISI 1015 steel
Young's modulus, GPa	204	216
Yield strength (a), MPa	370	550
Tensile strength, MPa	460	590
Elongation in 50 mm, %	27.7	4.5

(a) The yield stress based on 0.2% offset strain

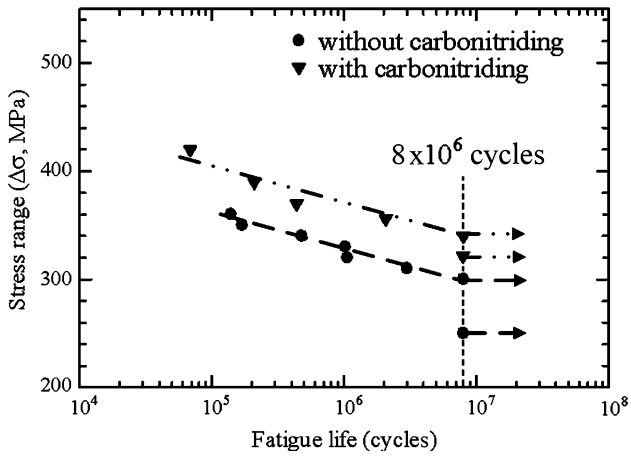

Fig. 6 Relationship between stress range and fatigue life

decreased with increasing depth, and became stable at approximately 1,000 μm depth. The magnitude of hardness at the core corresponded to the hardness of AISI 1015 steel without carbonitriding. At the location where the hardness value is 550 HV (Ref 18), the effective case depth for the present carbonitrided specimen was determined to be 400 μm.

The tensile tests of low-carbon steels with and without carbonitriding were performed three times. The Young's modulus was measured directly from the stress-strain curve. The variations of mechanical properties were <5%, and their averages were determined. The mechanical properties of AISI 1015 steels with and without carbonitriding are summarized in Table 2. Significant plastic deformation (percentage of elongation before fracture) could be observed for AISI 1015 steel without carbonitriding, i.e. ductile behavior, while the deformation of AISI 1015 steel with carbonitriding was controlled by carbonitrided layer and less plastic deformation was observed, i.e. brittle behavior. On the other hand, marginal difference of Young's modulus could be seen between AISI 1015 steels with and without carbonitriding. The elastic deformation relates to the strecthing of chemical bonds, while the plastic deformation occurs from the movement of atoms, i.e. dislocation. With the introduction of carbonitriding, the mobility of dislocation was limited, which resulted in the decrease of plastic deformation as well as the increases of yield strength and tensile strength.

The relationship between the residual stress in the longitudinal direction of fatigue specimen and distance from the surface of carbonitrided AISI 1015 steel is shown in Fig. 5. The compressive residual stress was high at the surface, decreased with increasing depth, and became stable tensile residual stress. The compressive residual stress at the surface was approximately 900 MPa, while the stable tensile residual stress was approximately 20 MPa. The transition from compressive residual stress to tensile residual stress occurred at approximately 400 μm, which corresponded to the effective case depth.

3.2 Stress-Fatigue Life Relationship

The fatigue tests of low-carbon steels with and without carbonitriding in each cyclic stress level were performed twice. The variation of number of cycles to failure was <10%, and their average numbers of cycles to failure were determined. The relationships between stress range and number of cycles to failure for AISI 1015 steels with and without carbonitriding on linear-log scale are shown in Fig. 6. The fatigue limit was defined as the stress range below which the number of cycles to failure was greater than 8×10^6 cycles. Both plots were linear with similar exponent; however, the fatigue lives of carbonitrided AISI 1015 steel were longer than those of AISI 1015 steel. The fatigue limits of specimens with and without carbonitriding were 340 and 300 MPa, respectively. Since the

compressive residual stress in the case layer of carbonitrided AISI 1015 steel could retard the propagation of nucleated crack, the fatigue life and fatigue limit of the present carbonitrided steel were, therefore, increased. Together with the improvement in wear resistance, i.e. the surface hardness increased about four times than that of AISI 1015 steel without carbonitriding (Fig. 4), the low-carbon steels treated by carbonitriding process could be used for engineering applications.

3.3 Effect of Residual Stress on Fatigue Resistance

Without any discontinuity at the case-core interface, the total strain (ε_{total}), strain of case (ε_{case}), and strain of core (ε_{core}) during cyclic loading were similar, while the applied stress in case ($\sigma_{app,case}$) and the applied stress in core ($\sigma_{app,core}$) were different due to the difference in mechanical properties. Schematic drawings of carbonitrided specimens without and with loading are shown in Fig. 7. The total strain (ε_{total}) and strain of core (ε_{core}) can be determined as follows,

$$\varepsilon_{total} = \sigma_{app,specimen}/E_{specimen} \quad \text{(Eq 1)}$$

$$\varepsilon_{core} = \sigma_{app,core}/E_{core} \quad \text{(Eq 2)}$$

where ($\sigma_{app,specimen}$) is the applied stress on specimen, ($\sigma_{app,core}$) is the applied stress on core material, $E_{specimen}$ is the Young's modulus of specimen, i.e. the carbonitrided AISI

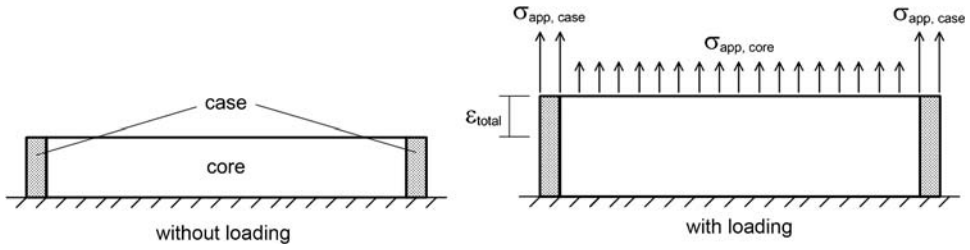

Fig. 7 Schematic drawings of carbonitrided AISI 1015 steels without and with loading

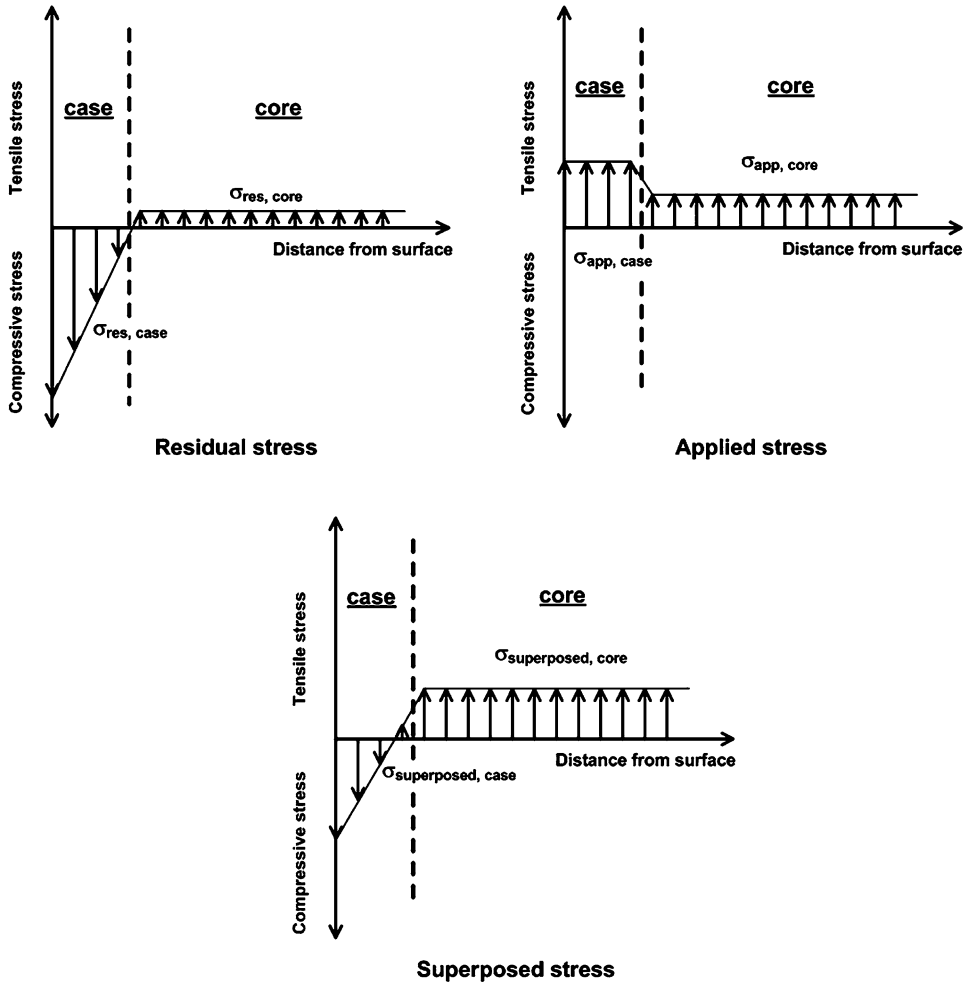

Fig. 8 Schematic drawings of the superposition (superposed stress) between residual stress and applied stress of carbonitrided AISI 1015 steel

1015 steel, and E_{core} is the Young's modulus of core material, i.e. the AISI 1015 steel. Based on the equivalence in strain between core and specimen, the applied stress on core ($\sigma_{app,core}$) could be estimated as follows,

$$\sigma_{app,core} = \sigma_{app,specimen} \cdot (E_{core}/E_{specimen}) \quad \text{(Eq 3)}$$

Since the applied load on specimen, and the summation between applied load on case and core were equal, the applied stress on case ($\sigma_{app,case}$) could be estimated as follows,

$$\sigma_{app,specimen} \cdot A_{specimen} = \sigma_{app,case} \cdot A_{case} + \sigma_{app,core} \cdot A_{core} \quad \text{(Eq 4)}$$

$$\sigma_{app,case} = (\sigma_{app,specimen} \cdot A_{specimen} - \sigma_{app,core} \cdot A_{core})/A_{case} \quad \text{(Eq 5)}$$

where $A_{specimen}$ is the area of specimen, A_{case} is the area of case material, and A_{core} is the area of core material.

The applied tensile stress on case material was suppressed by compressive residual stress, while that on core material was enhanced by tensile residual stress. Schematic drawings of the superposition between residual stress and applied stress, i.e. the superposed stress ($\sigma_{superposed}$), are shown in Fig. 8. The superposed stress in case material was compressive, while that in core material was tensile. The maximum tensile superposed stress was found not at the specimen surface but at the interface between the case and core materials. The applied stresses on specimens and the maximum tensile superposed stresses at the case-core interfaces are listed in Table 3. The maximum tensile superposed stresses at the case-core interfaces were lower than the applied stresses on the specimens. Thus, the fatigue resistance of carbonitrided AISI 1015 steel was higher than that of AISI 1015 steel, as shown previously in Fig. 6.

3.4 Fatigue Mechanisms

To understand the mechanism of fatigue crack initiation, a carbonitrided AISI 1015 fatigue specimen was cyclically loaded at the stress range of 420 MPa until 80% of fatigue life, sectioned, and then observed in an SEM. Micrographs of the sectioned specimen are shown in Fig. 9. Intergranular subsurface cracks were seen at approximately 400 μm below the surface, which corresponded to the location of maximum tensile superposed stress at the interface between the case and core materials. The chemical composition at the area of intergranular subsurface crack (Fig. 9b) has been analyzed using an energy dispersive spectroscopic technique (EDS, Oxford INCA 300). The main element was found to be iron, therefore a non-metallic inclusion was unlikely the cause of subsurface crack initiation. Since the compressive residual stress in case layer could prohibit the crack initiation while the tensile residual stress in core could enhance the fatigue process, the subsurface cracks nucleated at the case-core interface. The intergranular fracture at ambient temperature may occur due to various reasons, e.g. grain boundary corrosion, precipitation of brittle phases on grain boundary, and hydrogen embitterment (Ref 19). Since the present carbonitrided steel was direct-quenched, the segregation of phosphorus on grain boundaries and/or nucleation of cementite particles on grain boundaries would possibly occur (Ref 20, 21). This would cause the grain boundaries to become brittle and sensitive to fracture. Although the compressive residual stress within case layer could suppress

Table 3 Applied stresses, residual stresses, and superposed stresses of carbonitrided AISI 1015 specimens during fatigue tests

Applied stress on specimen, MPa	Applied stress on core material, MPa	Tensile residual stress in core material, MPa	Maximum tensile superposed stresses at case-core interface, MPa
340	301.6	20	321.6
360	319.3	20	339.3
370	328.2	20	348.2
390	345.9	20	365.9
420	372.5	20	392.5

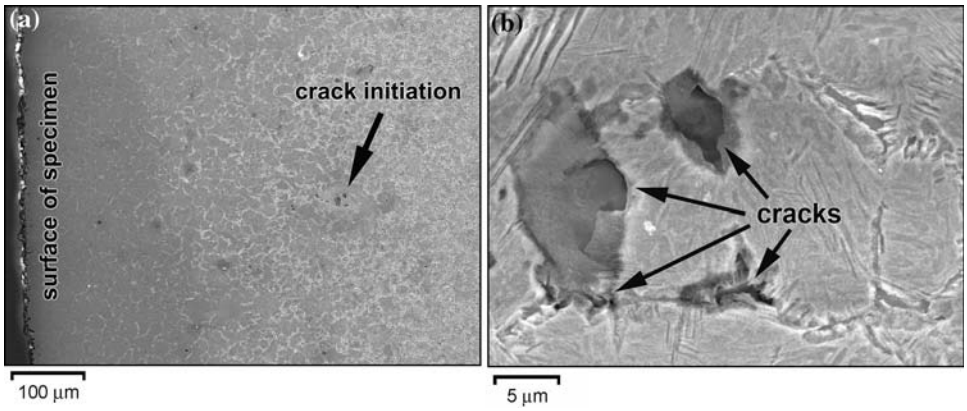

Fig. 9 SEM micrographs of subsurface cracks initiation at approximately 400 μm below the surface for the fatigue specimen tested at 420 MPa up to 80% of fatigue life; (a) low magnification, and (b) high magnification (loading was in vertical direction)

the propagation of subsurface cracks, the cracks eventually propagated after some incubation cycles. Similar observations were reported previously by Farfan et al. (Ref 8) for carburized AISI 8620 specimens under high-cycle fatigue.

The fracture surface of carbonitrided AISI 1015 steel after cyclically loading at the stress range of 420 MPa is shown in Fig. 10. In the case material, the subsurface cracks propagated under cyclic loading around the grain boundaries, which resulted in the intergranular fracture (Fig. 10b). On the other hand, the fatigue mechanism became fracture with crack-void interaction (elongated dimples) as crack propagated into core material (Fig. 10c). With the increasing of cracking area, the load bearing area decreased, crack propagation became unstable, and the final fracture occurred (Fig. 10d). At this stage, the fracture surface was composed of equiaxed dimples in various sizes, which represented the ductile fracture. The fatigue process is schematically shown in Fig. 11. After the initiation of subsurface cracks (stage I), some of them coalesced and became a long crack. With increasing the number of cycle, the subsurface crack propagated through the case layer (stage II), which was brittle and had lower fracture resistance than core material. After some incubation cycles, the subsurface crack reached the surface of specimen, and became a main crack (stage III). During this stage, the high stress around the crack tip caused the formation of voids in core material. In the final stage (stage IV), the static fracture occurred in the core

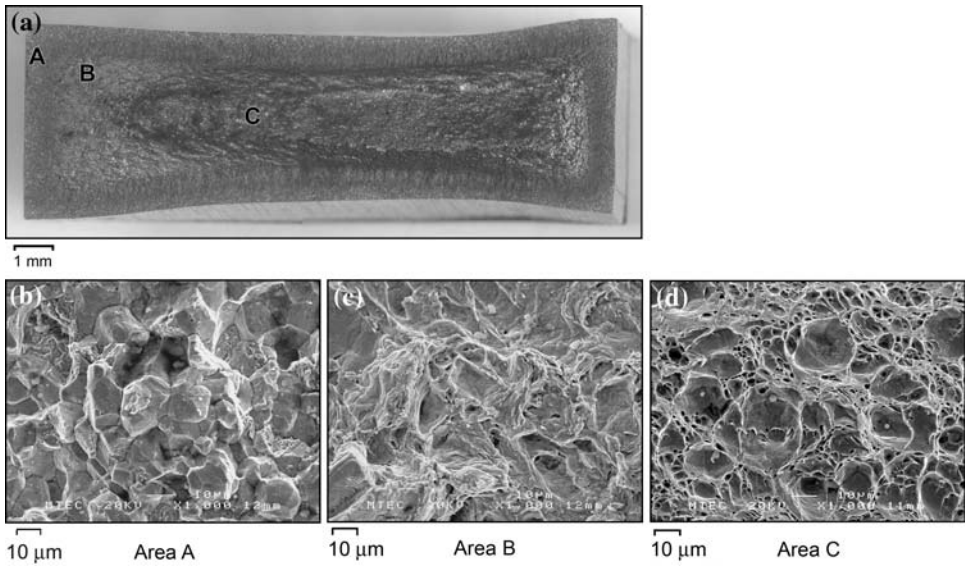

Fig. 10 SEM micrographs of fracture surface of carbonitrided AISI 1015 steel after fatigue test at stress range of 420 MPa; (a) total fracture surface, (b) fatigue in case material, (c) fatigue in core material, and (d) final fracture in core material

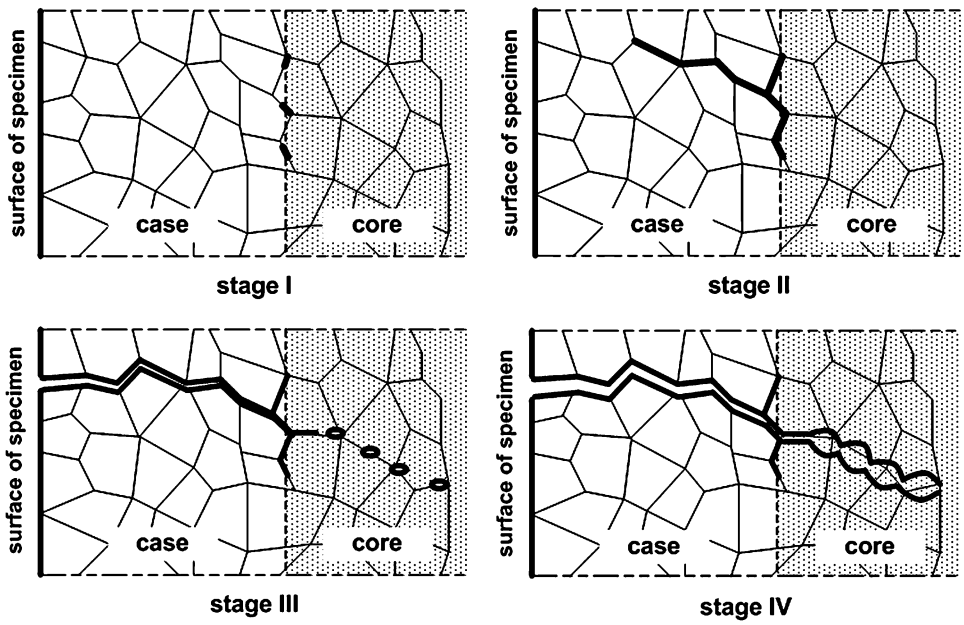

Fig. 11 Schematic drawings of the fatigue process of carbonitrided AISI 1015 steel (loading was in vertical direction)

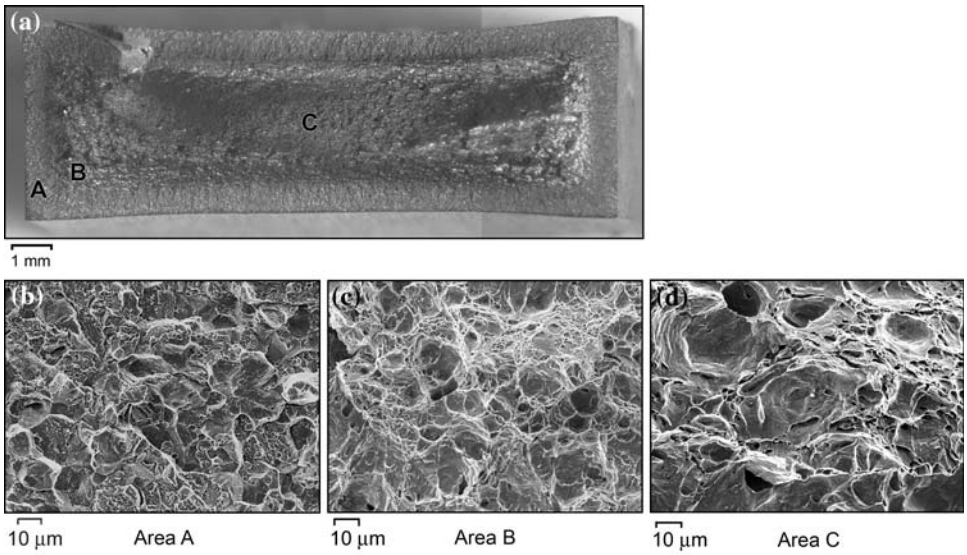

Fig. 12 SEM micrographs of fracture surface of carbonitrided AISI 1015 steel after tensile test; (a) total fracture surface, (b) fracture in case material, (c) fracture in core material, and (d) final fracture in core material

material, and consequently caused complete fracture. For comparison, the fracture surface of carbonitrided AISI 1015 steel after tensile test is shown in Fig. 12. Unlike the fracture surface of fatigue specimens, the crack initiated from the surface and then propagated through the case layer in both intergranular and transgranular manners (Fig. 12b). However, the fracture surface of tensile specimen became similar to that of fatigue specimen when the crack propagated through core material (Fig. 12c, d).

It is known that the fatigue resistance of steel could be influenced by microstructure (Ref 22) and chemical composition (Ref 23). In the present work, the tempered martensite was observed in the case layer of low-carbon steel with carbonitriding (Fig. 3), and the differences in chemical composition between low-carbon steels with and without carbonitriding were observed at their surfaces (Table 1). However, no significant difference in chemical composition was detected between the core of low-carbon steel with carbonitriding and the bulk of low-carbon steel without carbonitriding. Since the subsurface cracks in the present carbonitrided steel initiated and propagated in the intergranular manner below the surface, the tempered martensite within grains and the chemical composition at the surface were unlikely the principal reasons for fatigue improvement.

4. Conclusions

The effect of residual stress on fatigue behavior and mechanisms of carbonitrided AISI 1015 steel under uniaxial cyclic loading has been experimentally studied. The main conclusions obtained are as follows:

(1) By progressive removal of thin surface layers using an electropolishing technique, and subsequent residual stress measurements using an x-ray diffraction technique, the compressive residual stress at the surface was approximately 900 MPa. The stress decreased toward the center, and became stable tensile residual stress of approximately 20 MPa.

(2) With the introducing of compressive residual stress, the fatigue resistance of carbonitrided AISI 1015 steel was higher than that of AISI 1015 steel without carbonitriding. The fatigue limits of AISI 1015 steels with and without carbonitriding were 340 and 300 MPa, respectively.

(3) Subsurface cracks initiated at the transition between the compressive residual stress in case material to the tensile residual stress in core material, i.e. the case-core interface at approximately 400 μm below the surface. With increasing the number of cycles, the subsurface cracks coalesced and propagated intergranularly through the case layer. After some incubation cycles, the subsurface crack reached the surface of specimen, and became a main crack. During this stage, the stress increased, and caused the formation of voids in core material. Consequently, the crack propagated through the core material, interacted with voids, and caused complete fracture.

Acknowledgments

The authors would like to acknowledge the discussions and supports from Prof. Y. Mutoh (Nagaoka University of Technology, Japan), Mr. N. Taweejun (Thai Tohken Thermo Co., Ltd.), Mr. S. Chaiyana, the Thailand Research Fund (TRF), the National Research Council of Thailand (NRCT), the Commission on Higher Education of Thailand, the Scientific and Technological Research Equipment Centre of Chulalongkorn University (STREC), and the National Metal and Materials Technology Center (MTEC).

References

1. D. Croccolo, L. Cristofolini, M. Bandini, and A. Freddi, Fatigue Strength of Shot-Peened Nitrided Steel: Optimization of Process Parameters by Means of Design of the Experiment, *Fatigue Fract. Eng. Mater. Struct.*, 2002, **25**(7), p 695–707
2. C.S. Montross, T. Wei, L. Ye, G. Clark, and Y.W. Mai, Laser Shock Processing and its Effects on Microstructure and Properties of Metal Alloys: A Review, *Intl. J. Fatigue*, 2002, **24**(10), p 1021–1036

3. R. Ahmed and M. Hadfield, Mechanisms of Fatigue Failure in Thermal Spray Coatings, *J. Thermal Spray Technol.*, 2002, **11**(3), p 333–349
4. M. Widmark and A. Melander, Effect of Material, Heat Treatment, Grinding and Shot Peening on Contact Fatigue Life of Carburised Steels, *Intl. J. Fatigue*, 1999, **21**(4), p 309–327
5. *ASM Handbook, Volume 4: Heat Treating*, J.R. Davis, Ed., ASM International, OH, 1994
6. R.I. Stephens, A. Fatemi, R.R. Stephens, and H.O. Fuchs, *Metal Fatigue in Engineering*. 2nd ed., Wiley-Interscience Publication, New York, 2001
7. J.A. Collins, *Failure of Materials in Mechanical Design: Analysis, Prediction, Prevention*. 2nd ed., John Wiley & Sons, New York, 1993
8. S. Farfan, C. Rubio-Gonzalez, T. Cervantes-Hernandez, and G. Mesmacque, High Cycle Fatigue, Low Cycle Fatigue and Failure Modes of a Carburized Steel, *Intl. J. Fatigue*, 2004, **26**(6), p 673–678
9. M. Karadag and R.I. Stephens, The Influence of High R Ratio on Unnotched Fatigue Behavior of 1045 Steel with Three Different Heat Treatments, *Intl. J. Fatigue*, 2003, **25**(3), p 191–200
10. A.J. McEvily, K. Pohl, and P. Mayr, Comparison of the Fractographic Features of a Carburized Steel Fractured Under Monotonic or Cyclic Loading, *Mater. Charact.*, 1996, **36**(4–5), p 153–157
11. K. Genel, M. Demirkol, and M. Capa, Effect of Ion Nitriding on Fatigue Behaviour of AISI 4140 Steel, *Mater. Sci. Eng. A*, 2000, **279**(1–2), p 207–216
12. M. Przylecka, W. Gestwa, and M. Kulka, Influence of Carbonitriding and Heat Treatment on the Properties of Low- and High-Carbon Steels, *Mater. Sci. Forum*, 1994, **163–6**(Pt. 1), p 239–244
13. ASTM E466-96: Conducting Force Controlled Constant Amplitude Axial Fatigue Tests of Metallic Materials, Volume 3.01, *Annual Book of ASTM Standards*, 1996
14. STM E1558-93: Electrolytic Polishing of Metallographic Specimens, Volume 3.01, *Annual Book of ASTM Standards*, 1996
15. ASTM E384-89: Microhardness of Materials, Volume 3.01, *Annual Book of ASTM Standards*, 1996
16. ASTM E8M-96: Tension Testing of Metallic Materials, Volume 3.01, *Annual Book of ASTM Standards*, 1996
17. *ASM Handbook, Volume 1: Properties and Selection: Irons, Steels, and High-Performance Alloys*, J.R. Davis, Ed., ASM International, OH, 1994
18. K. Genel, Estimation Method for the Fatigue Limit of Case Hardened Steels, *Surface Coat. Technol.*, 2005, **194**(1), p 91–95
19. S. Suresh, *Fatigue of Materials*. 2nd ed., Cambridge University Press, New York, 1998
20. T. Ando and G. Krauss, The Effect of Phosphorus Content on Grain Boundary Cementite Formation in AISI 52100 Steel, *Metal. Trans. A*, 1981, **12A**, p 1283–1290
21. G. Krauss, Microstructure and Fracture of a Carburized Steel, *Metal. Trans. A*, 1978, **9A**(11), p 1527–1535
22. S Sankaran, V Subramanya Sarma, K.A. Padmanabhan, G Jaeger, and A. Koethe, High Cycle Fatigue Behaviour of a Multiphase Microalloyed Medium Carbon Steel: A Comparison Between Ferrite-Pearlite and Tempered Martensite Microstructures, *Mater. Sci. Eng. A*, 2003, **362**(1–2), p 249–256
23. M.R. Green, W.M. Rainforth, M.F. Frolish, and J.H. Beynon, The Effect of Microstructure and Composition on the Rolling Contact Fatigue Behaviour of Cast Bainitic Steels, *Wear*, 2007, **263**(1–6), p 756–765